Prediction of Precombustion Wall Pressure Distributions in Scramjet Engines

P. J. WALTRUP* AND F. S. BILLIG†
Johns Hopkins University, Applied Physics Laboratory, Silver Spring, Md.

Nomenclature

A = area
D = diameter of duct
ER = fuel-air equivalence ratio
M = Mach number
p = pressure
Re_θ = Reynolds number based on initial boundary-layer momentum thickness
s = axial coordinate with origin at beginning of precombustion-shock pressure rise; $\bar{s} = s/(s_0 + s_d)$; $s_t = s_0 + s_d$
s_d, s_0 = displacements of interaction region downstream and upstream of fuel injector, respectively
T = temperature
$\bar{\varepsilon}$ = value of exponent in pressure-area relationship
η_c = combustion efficiency
θ = boundary-layer momentum thickness

Subscripts

a = combustor entrance
f = final pressure
s = condition following shock
t_0, t_f = total, plenum condition of air and fuel, respectively
w = condition at wall

Introduction

DURING the past several years, considerable attention has been given to the supersonic combustion ramjet (scramjet) engine because it is potentially the most efficient engine cycle in the Mach 6-15 speed range.[1,2] In Ref. 3 a pseudo-one-dimensional model of the engine cycle was developed which showed that, for typical operating conditions, combustion must be preceded by a compression wave structure. In addition, this model permits the a priori prediction of the strength of the precombustion shock structure, the axial pressure distribution downstream of the shock structure, and the flow properties in the combustor exit plane. However, the definition of the pressure field and attendant separation zone in the precombustion-shock interaction region (Fig. 1a) has been imprecise. In Ref. 4, an initial attempt was made to model these features, which are important because of the possibility of severe interaction with the inlet's flowfield. However, at that time, the quantity of experimental data available from combustor tests was so limited that the general applicability of the semiempirical model of this region could not be evaluated.

Subsequent to the publication of Ref. 4, additional data have been generated in a simple, nonreacting system which produces shock structures and shock/boundary-layer interactions analogous to those present at the entrance of supersonic combustors (Fig. 1b).[5] The data were obtained in cylindrical ducts where throttling or overexpansion, rather than combustion, is the cause of the compression. In either case, the supersonic flow must negotiate an over-all pressure rise via a multiple shock-expansion process. These tests included all first-order effects (other than nonconstant-area combustor geometry) on the shock structure, viz., Mach number (M_a), Reynolds number (Re_θ), duct diameter (D), and boundary-layer momentum thickness (θ), and were used to derive a semi-emprical equation which describes the extent of the precombustion shock region (s_t) as well as its wall static pressure distribution [$p_w(s)$] for given initial conditions and over-all pressure ratio (p_f/p_a). The purpose of this Note is to use this data correlation to redefine the semi-empirical model presented in Ref. 4 and compare the two to results from direct-connect combustor tests.

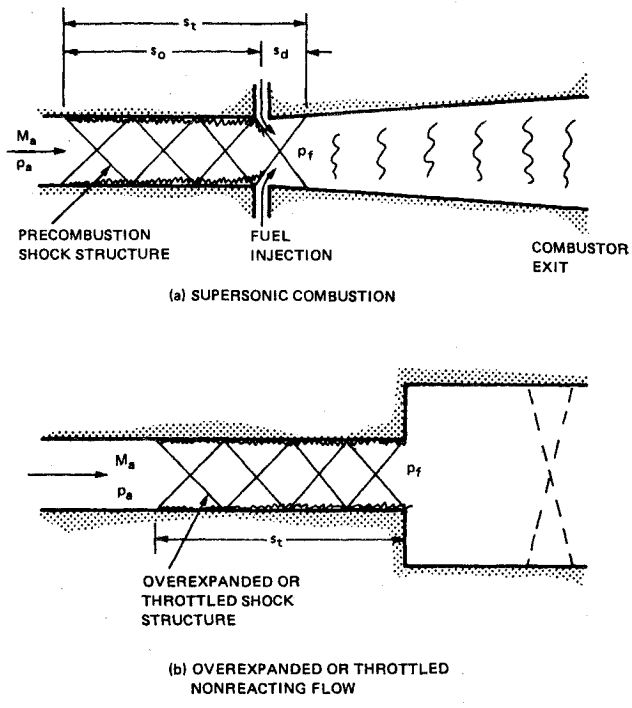

Fig. 1 Schematic illustration on flow structures.

The Previous Model and the Revised Model

The limited data presented in Ref. 4 indicated that the precombustion shock structure extended both upsteam (s_0) and downstream (s_d) of the fuel injector, and it was assumed that the pressure distribution was generally s-shaped in character. Accordingly

$$p_w/p_a = 1 + 3(p_{s_d}/p_a - 1)\bar{s}^2 + 2(1 - p_{s_d}/p_a)\bar{s}^3 \qquad (1)$$

was chosen to represent the wall pressure distribution where

$$p_{s_d}/p_a = (A_a/A_{s_d})^{\bar{\varepsilon}/(\bar{\varepsilon}-1)}(p_s/p_a) \qquad (2)$$

and A_{s_d} is the combustor cross-sectional area at s_d. The value of $\bar{\varepsilon}$ is obtained from the basic process analysis of Ref. 3 together with the mainstream pressure rise p_s/p_a of the precombustion shock structure. The functional forms selected for s_0 and s_d were

$$s_d/\theta = 35(p_s/p_a); \quad s_0/\theta = 35(p_{s_d}/p_a)^2 \qquad (3)$$

where the selection of θ as the nondimensionalizing parameter was somewhat arbitrary due to the limited data available. On the other hand, the new data from Ref. 5 were obtained over a significant range of initial conditions and the correlation

$$\frac{s_t(M_a^2 - 1)Re_\theta^{1/4}}{D^{1/2}\theta^{1/2}} = 50\left(\frac{p_{s_d}}{p_a} - 1\right) + 170\left(\frac{p_{s_d}}{p_a} - 1\right)^2 \qquad (4)$$

Presented, in part, as Paper 72-1181 at the AIAA/SAE 8th Propulsion Joint Specialist Conference, New Orleans, La., November 29–December 1, 1972; submitted April 9, 1973. This work was supported by the U.S. Navy under Naval Ordnance Systems Command Contract N00017-72-C-4401.

Index categories: Airbreathing Propulsion, Hypersonic, Nozzle and Channel Flow; Shock Waves and Detonations.

* Engineer, Hypersonic Ramjets Project. Associate Member AIAA.

† Supervisor, Hypersonic Ramjets Project. Associate Fellow AIAA.

gives a good definition of $s_t = s_0 + s_d$. Moreover $p_w(s)$ can be obtained by replacing s_t by s and p_{s_d}/p_a by p_w/p_a. To apply this new correlation to combustor flows, it is necessary to relate the location of the injector relative to either the upstream or downstream extent of the pressure rise curve. Based on the following heuristic arguments, a modified expression for s_d is retained which, with Eq. (4), is used to obtain s_0 and $p_w(s)$, thus eliminating Eqs. (1) and (3). Since combustion represents a "blockage" to the incoming supersonic flow equivalent to the case of a throttle in nonreacting flow, and since the effective location of this blockage is governed by some characteristic of the injection-combustion process, e.g., the "ignition delay" distance, s_d should be a combustion-related parameter which presumably could include geometric effects. However, since the combustor data[4] are limited, it is inappropriate to include additional functional dependencies in the expression for s_d other than changing the dimensional scaling factor to $D^{1/2}\theta^{1/2}$ to be consistent with Eq. (4) and recognizing the obvious limit $s_d = 0$ for $p_s/p_a = 1$. The expression then becomes

$$s_d/(D^{1/2}\theta^{1/2}) = 0.5(p_s/p_a - 1) \qquad (5)$$

where the constant (0.5) is consistent with the data of Ref. 4.

The procedure for relating this revised model to a given combustor may now be summarized as follows: a) determine p_s/p_a and $\bar{\varepsilon}$ from the basic combustor process analysis of Ref. 3; b) determine s_d from Eq. (5); c) determine A_{s_d} for the given combustor geometry at station s_d; d) determine p_{s_d}/p_a from Eq. (2); e) using p_{s_d}/p_a in Eq. (4), determine $s_t(= s_0 + s_d)$. Also use Eq. (4) to determine the shape of the pressure rise curve $p_w(s)$.

Comparison with Direct-Connect Combustor Test Results

Schematics of the direct-connect combustor tests with hydrogen fuel reported in Ref. 4 are shown in Figs. 2–4 along with their respective wall pressure distributions and inlet conditions. In each case, M_a, θ, D, and combustor inlet-to-exit area ratio, are 3.23, 0.0146 in., 2.74 in., and 2.0, respectively. The computed wall pressure distributions based on the revised method are shown as the solid curves in Figs.

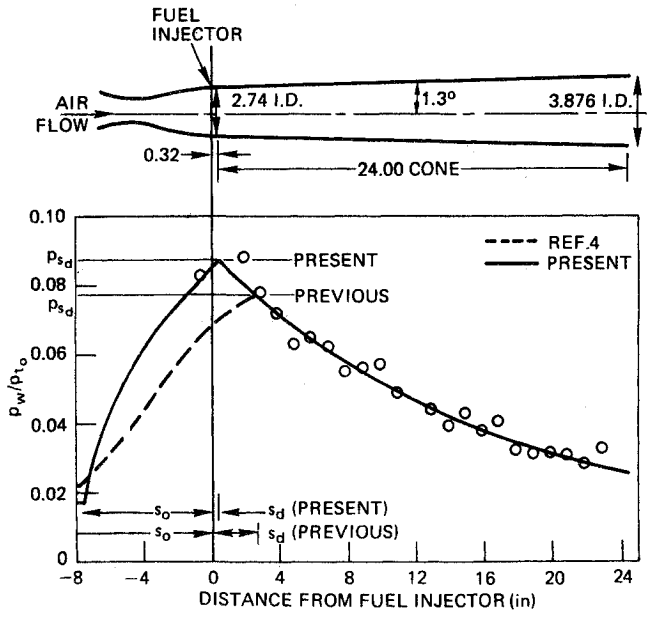

T_{t_o} °R	P_{t_o} psia	T_a °R	P_a psia	T_{t_f} °R	ER	η_c
O 4000	449	1515	7.36	516	0.80	0.572

Fig. 2 Comparison of theoretical and experimental wall pressure distributions in a conical combustor.

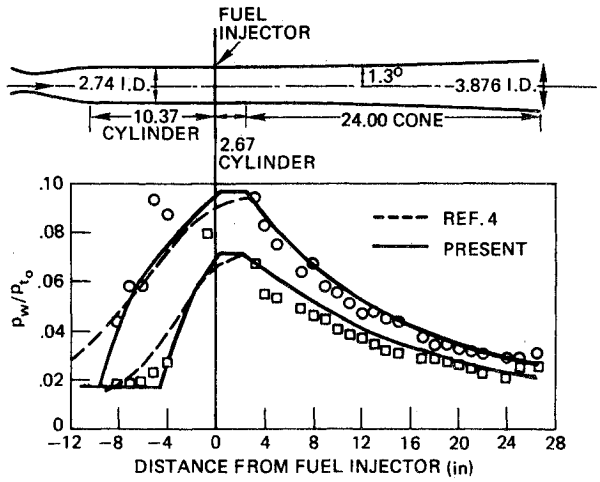

T_{t_o} °R	P_{t_o} psia	T_a °R	P_a psia	T_{t_f} °R	ER	η_c
O 4135	456	1581	7.52	1158	0.78	0.81
□ 4150	456	1590	7.52	1160	0.49	0.92

Fig. 3 Comparison of theoretical and experimental wall pressure distributions in a short-cylinder-cone combustor.

2–4 and those based on Eqs. (1–3) are shown as dashed curves. In Fig. 2, a conical combustor is close-coupled to the nozzle, and only one upstream data point is available. The computed s_d of 0.44 in. places s_d slightly within the conical section, so that p_{s_d}/p_a is lower than p_s/p_a (5.25 vs 5.40), and s_0 is 7.76 in. Here the new model provides a better match to the experimental peak pressure and closely approximates the one upstream data point. For the short-cyl-cone combustor Fig. (3), the values of s_d are 0.46 in. and 0.35 in. for $ER = 0.78$ and 0.49, respectively, so that s_d, in both cases, still lies in the constant-area section, and p_{s_d} equals the midstream shock pressure p_s. For both ER's the revised model more nearly approximates the slope of the pressure rise data and the maximum pressure reached, as well as s_0. For the step-cyl-cone combustor (Fig. 4), the values of p_{s_d}/p_a corresponding to $A_{s_d}/A_a = 1.44$ are 2.32 and 3.17 for $ER = 0.51$ and 0.93, respectively. Again, the levels of p_{s_d} in the cylindrical section are closely approximated, and the new model describes

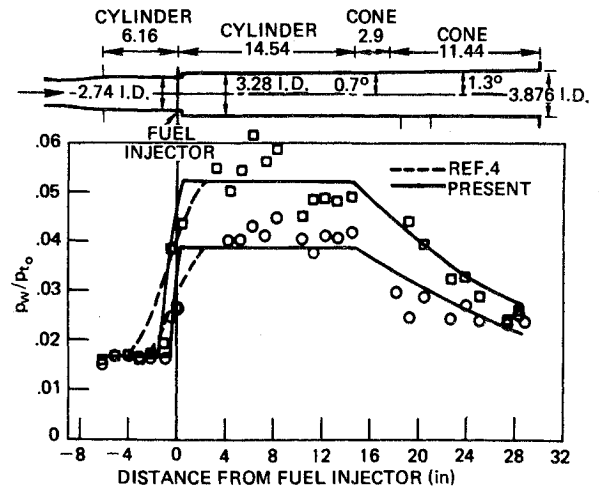

T_{t_c} °R	P_{t_c} psia	T_a °R	P_a psia	T_{t_f} °R	ER	η_c
3875	446	1452	7.32	1126	0.93	0.68
3970	450	1500	7.43	1185	0.51	0.89

Fig. 4. Comparison of theoretical and experimental wall pressure distributions in a step-cylinder-cone combustor.

better the upstream propagation of the precombustion shock and its wall pressure distribution.

These comparisons show that the new model provides better descriptions of the wall pressure distributions and the over-all shock pressure rises for the available test data. Further testing is needed to determine whether more complex expressions for s_d will be needed if the combustor inlet conditions are significantly changed.

References

[1] Dugger, G. L., "Comparison of Hypersonic Ramjet Engines with Subsonic and Supersonic Combustion," Fourth AGARD Colloquium, Milan, Italy; also *Combustion and Propulsion-High Mach Number Air Breathing Engines*, edited by Jaumotte, Rothrock, and Le Febvre, Pergamon Press, New York, 1960.

[2] Ferri, A., "Review of Scramjet Technology," *Journal of Aircraft*, Vol. 5, No. 1, Jan. 1968, pp.3–10.

[3] Billig, F. S. and Dugger, G. L., "The Interaction of Shock Waves and Heat Addition in the Design of Supersonic Combustors," *Twelfth Symposium (International) on Combustion*, The Combustion Inst., Pittsburgh, Pa. 1969, pp. 1125–1139.

[4] Billig, F. S., Dugger, G. L., and Waltrup, P. J., "Inlet-Combustor Interface Problems in Scramjet Engines," *The First International Symposium on Air Breathing Propulsion*, Marseille, France, June 1972.

[5] Waltrup, P. J. and Billig, F. S., "The Structure of Shock Waves in Cylindrical Ducts," *AIAA Journal*, Vol. 11, No. 10, Oct. 1973, pp. 1404–1408.

Correlation of Hypersonic Zero-Lift Drag Data

JOHN J. REHDER*
NASA Langley Research Center, Hampton, Va.

Nomenclature

$(C_{D,l^2})_{min}$ = minimum or zero-lift drag coefficient, based on length squared
C'_∞ = Chapman-Rubesin viscosity coefficient, $[(T_\infty/T')\mu'/\mu_\infty]$
l = model length
M = Mach number
n = power law exponent
P = pressure
$Re_{\infty,l}$ = freestream Reynolds number based on model length
T = temperature
$\bar{V}'_\infty$ = viscous correlation parameter, $M_\infty(C'_\infty/Re_{\infty,l})^{1/2}$
x = longitudinal coordinate with origin at body nose
y = lateral coordinate with origin at body centerline
μ = viscosity
γ = ratio of specific heats

Subscripts
∞ = freestream conditions
T = stagnation conditions

Superscripts
$( )'$ = based on reference temperature conditions (Ref. 5)

Introduction

HYPERSONIC wind-tunnel testing in support of basic research or application programs such as the Shuttle during the past few years has focused attention on the need for properly correlating force data taken under varying test conditions. This Note demonstrates the applicability of one correlation parameter for drag coefficients. The present investigation, part of a more comprehensive study, demonstrates correlation of zero-lift drag coefficients of several simple shapes measured at $M = 10.03$ in air and at $M = 20$ in helium with the theoretical inviscid values.

Received May 18, 1973.
Index categories: LV/M Aerodynamics; Entry Vehicle Testing.
* Aerospace Technologist, Operations Analysis Section, Vehicle Analysis Branch, Space Systems Division. Member AIAA.

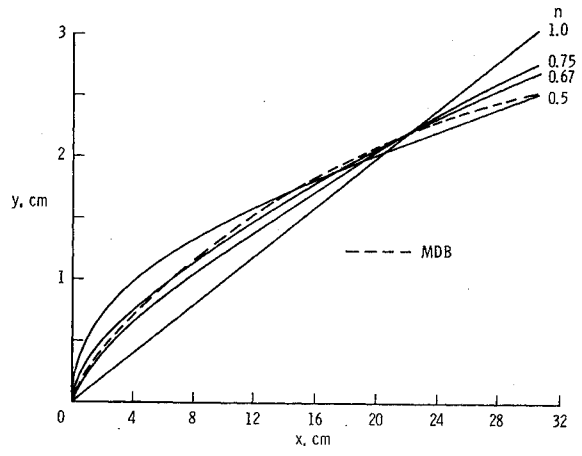

Fig. 1 Comparison of test model planforms.

Tests and Analysis

The shapes tested were a series of power-law bodies [$y = y_{max}(x/l)^n$] and a theoretical minimum drag body (MDB). All bodies had circular cross sections and were constrained to the same length and volume. A comparison of the contours of the bodies is shown in Fig. 1 with the vertical scale expanded to emphasize the differences. These bodies are described in more detail in Ref. 1 and 2.

The inviscid values of $(C_{D,l^2})_{min}$ were obtained by the method of characteristics using a 45° conical nose to initiate the calculations. Zero-lift drag coefficient is based on model length squared since both planform area and base area vary from model to model due to the length-volume constraint.

The experimental data were obtained in the 22-in. Helium Tunnel and the 15-in. Hypersonic Flow Tunnel at the Langley Research Center. Except for the minimum drag shape in the 22-in. Helium Tunnel, all of the data have been previously published.[1,2] The test conditions for all of the tests are presented in Table 1.

An attempt to correlate the zero-lift drag data obtained in these facilities with inviscid values using the parameter $M_\infty(Re_{\infty,l})^{-1/2}$ (Fig. 2) was unsuccessful, although this parameter has been used with success in the past[3] to correlate hypersonic data from air tunnels at similar temperatures. The parameter did correlate the $M = 20$ data and the inviscid results linearly, while the $M = 10.03$ data are considerably above the correlation curves. Apparently, general correlation requires that the wide variations in test temperatures and possible variations due to differences in the ratios of specific heat be considered.

Table 1 Test conditions

Test	M_∞	$Re_{\infty,l}$	P_T, N/m²	T_T, °K	Facility
Present investigation and Ref. 2	18.1	1.65×10^6	2.2×10^6	306.5	22-in. Helium Tunnel
	19.0	2.50×10^6	3.6×10^6	305.4	
	20.3	4.40×10^6	7.0×10^6	307.6	
	21.6	8.00×10^6	13.9×10^6	303.2	
Ref. 1	10.0	1.4×10^6	6.9×10^6	1000.0	15-in. Hypersonic Flow Tunnel